How Efficient Are the Hydrido-Bridged Diplatinum Catalysts in the Hydrosilylation, Hydrocyanation, and Hydroamination of Alkynes: A Theoretical Analysis of the Catalytic Cycles Employing Electronic Structure Calculation Methods

Constantinos A. Tsipis* and Christos E. Kefalidis

Laboratory of Applied Quantum Chemistry, Faculty of Chemistry, Aristotle University of Thessaloniki, 541 24 Thessaloniki, Greece

Received October 31, 2005

A comprehensive and consistent picture of the catalytic cycle of hydrosilylation, hydrocyanation, and hydroamination of ethyne catalyzed by hydrido-bridged diplatinum complexes has been derived by means of electronic structure calculations at the B3LYP and CCSD(T) levels of theory, using the LANL2DZ+BSII(Pt)∪6-31G**(L) basis set. All crucial reaction steps of the entire catalytic courses have been scrutinized. Three critical steps of the catalytic cycles corresponding to (i) the hydride migration to the acceptor C atom of the coordinated ethyne substrate, (ii) the reductive elimination of the final product, and (iii) the oxidative addition process that regenerates the catalytic species were found to be the rate-limiting steps with activation barriers ($\Delta E_{CCSD(T)}^{\ddagger}$) of 11.6, 5.1, and 7.1 kcal/mol for the hydrosilylation, 6.9, 24.9, and 1.6 kcal/mol for the hydrocyanation, and 10.5, 35.4, and 25.5 kcal/mol for the hydroamination reactions. Overall, all catalytic processes are predicted to be exothermic with exothermicities of −32.1 (−25.5), −37.8 (−28.2), and −53.7 (−45.1) kcal/mol for the hydrosilylation, hydrocyanation, and hydroamination of ethyne, respectively, at the B3LYP (CCSD(T)) levels of theory. From the detailed analysis of both the thermodynamic and kinetic aspects of the catalytic cycles it can be inferred that the catalytic efficiency of the hydrido-bridged diplatinum complexes follows the trend hydrocyanation ≥ hydrosilylation > hydroamination.

Introduction

Several years ago[1] we found that the hydrido-bridged diplatinum complexes $[\{Pt(SiR'_3)(\mu\text{-}H)[P(cyclo\text{-}C_6H_{11})_3]\}_2]$ resulting from the reaction of the $[Pt(C_2H_4)_2\{P(cyclo\text{-}C_6H_{11})_3\}]$ complexes with hydrosilanes, $HSiR'_3$ ($SiR'_3 = SiCl_3$, $SiClMe_2$, $SiMe_2Ph$, $SiMe_2(CH_2Ph)$, $SiMe_2Et$, $SiEt_3$, or $Si(OEt)_3$) and their precursors $[Pt(C_2H_4)_2(PR_3)]$, both containing only one phosphane ligand per metal center, are superior catalysts to the platinum species used previously.[2,3] Yields of hydrosilylation products are generally greater using the $[\{Pt(SiR'_3)(\mu\text{-}H)[P(cyclo\text{-}C_6H_{11})_3]\}_2]$ catalysts than with other complexes of group 8,[4] for example, H_2PtCl_6,[2,5] $[Fe(CO)_5]$,[6] $[\{PtCl(\mu\text{-}Cl)C_2H_4)\}_2]$,[7] various triphenylphosphine-Pt(0) d^{10} complexes,[8] $[RhCl(Ph_3P)_3]$,[9] or metallic platinum.[2,5] Adding hydrosilanes to double or triple carbon−carbon bonds usually proceeds exothermally immediately on mixing the reactants at room temperature in a catalyst:substrate ratio in the range of 10^{-4} to 10^{-6}:1. Hydrosilylation of unsaturated organic compounds is a key catalytic reaction for production of industrially important products, since organosilicon compounds are useful as an intermediate in organic synthesis, dendrimers, and polymer chemistry.[10] Despite the lack of kinetic information on the hydrosilylation of alkynes catalyzed by the diplatinum complexes, a possible mechanism conforming to the well-established Chalk−Harrod mechanism[7] has been suggested.[1d,e] (Scheme 1).

According to the proposed mechanism, the first step of the hydrosilylation reaction involves the cleavage of the hydrido-bridges in the diplatinum complexes promoted by the incoming

* To whom correspondence should be addressed. E-mail: tsipis@chem.auth.gr.

(1) (a) Green, M.; Howard, J. A. K.; Proud, J.; Spencer, J. L.; Stone, F. G. A.; Tsipis, C. A. *J. Chem. Soc., Chem. Commun.* **1976**, 671−672. (b) Ciriano, M.; Green, M.; Howard, J. A. K.; Proud, J.; Spencer, J. L.; Stone, F. G. A.; Tsipis, C. A. *J. Chem. Soc., Dalton. Trans.* **1976**, 801−808. (c) Ciriano, M.; Green, M.; Howard, J. A. K.; Murray, M.; Spencer, J. L.; Stone, F. G. A.; Tsipis, C. A. *Advances in Chemistry Series No 167*; American Chemical Society: Washington, DC, 1976; pp 112−121. (d) Green, M.; Spencer, J. L.; Stone, F. G. A.; Tsipis, C. A. *J. Chem. Soc., Dalton Trans.* **1977**, 1519−1524. (e) Green, M.; Spencer, J. L.; Stone, F. G. A.; Tsipis, C. A. *J. Chem. Soc., Dalton Trans.* **1977**, 1525−1529. (f) Tsipis, C. A. *J. Organomet. Chem.* **1980**, *187*, 427−446. (g) Tsipis, C. A. *J. Organomet. Chem.* **1980**, *188*, 53−61.

(2) (a) Speier, J. L.; Webster, J. A.; Barnes, G. H. *J. Am. Chem. Soc.* **1957**, *79*, 974−979. (b) Saam, J. C.; Speier, J. L. *J. Am. Chem. Soc.* **1958**, *80*, 4104−4106. (c) Ryan, J. W.; Speier, J. L. *J. Am. Chem. Soc.* **1964**, *86*, 895−898.

(3) (a) Benkeser, R. A.; Hickner, R. A. *J. Am. Chem. Soc.* **1958**, *80*, 5298−5300. (b) Benkeser, R. A.; Burrous, M. L.; Nelson, L. E.; Swisher, J. V. *J. Am. Chem. Soc.* **1961**, *83*, 4385−4389.

(4) Cundy, C. S.; Kingstom, B. M.; Lappert, M. F. *Adv. Organometallic Chem.* **1973**, *11*, 253.

(5) Musolf, M. C.; Speier, J. F. *J. Org. Chem.* **1964**, *29*, 2519.

(6) Chukovskaya, E. Ts.; Kuzmina, N. A.; Rozhkova, M. I. *Zh. Obshchei Khim.* **1966**, *36*, 2165.

(7) Chalk, A. J.; Harrod, J. F. *J. Am. Chem. Soc.* **1965**, *87*, 16.

(8) (a) Fink, W. *Helv. Chim. Acta* **1971**, *54*, 1304. (b) Yamamoto, K.; Hayashi, J.; Kumada, M. *J. Organomet. Chem.* **1971**, *28*, C37.

(9) (a) Chalk, A. J. *J. Organomet. Chem.* **1970**, *21*, 207. (b) Haszeldine, R. N.; Parish, R. V.; Parry, D. J. *J. Chem. Soc. (A)* **1969**, 683.

(10) (a) Speier, J. L. *Adv. Organomet. Chem.* **1979**, *17*, 407. (b) Speier, J. L. *Adv. Organomet. Chem.* **1979**, *17*, 407. (c) Harrod, J. F.; Chalk, A. J. In *Organic Synthesis via Metal Carbonyls*; Wender, I., Pino, P., Eds.; Wiley: New York, 1979; Vol. 2, p 673. (d) Tilley, T. D. In *The Chemistry of Organic Silicon Compounds*; Patai, S., Rappoport, Z., Eds.; Wiley: New York, 1989; p 1415. (e) Ojima, I. In *The Chemistry of Organic Silicon Compounds*; Patai, S., Rappoport, Z., Eds.; Wiley: New York, 1989; p 1479. (f) Ohsima, K. In *Advances in Metal-Organic Chemistry*; Liebeskind, L. S., Ed.; JAI Pres Ltd.: London, 1991; Vol. 2, p 101.

10.1021/om0509342 CCC: $33.50
Publication on Web 03/01/2006

Scheme 1. Proposed Catalytic Cycle for the Hydrosilylation of Alkynes Catalyzed by Hydrido-Bridged Diplatinum Complexes

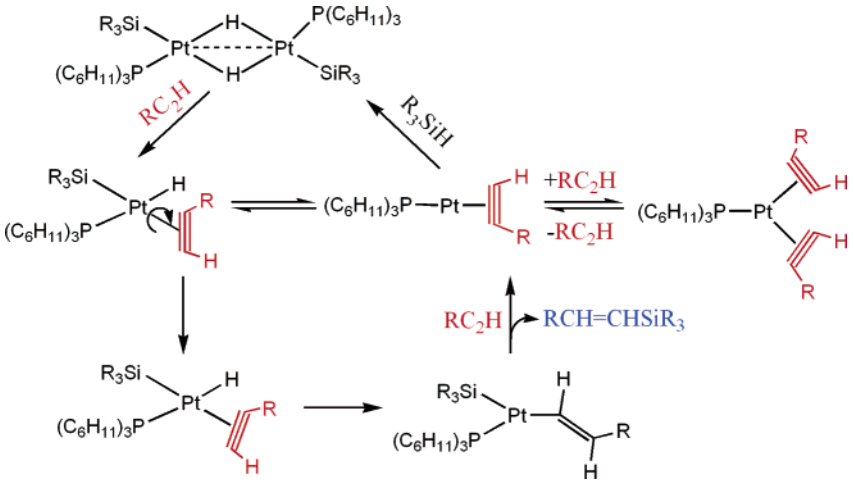

alkyne substrate, thus affording a square planar mononuclear Pt(II) intermediate with the coordinated alkyne molecule in *trans* position with respect to the silyl ligand. The next step involves rotation of the alkyne into the coordination plane, followed by migration of the hydride from Pt to an acetylenic carbon with formation of a Pt(II) vinyl complex. Reductive migration of the silyl group from the metal to carbon would then regenerate the Pt(0) catalyst.

Considering the high catalytic activity and regioselectivity of the hydrido-bridged diplatinum complexes in hydrosilylation reactions, we explored their catalytic activity in two other catalytic reactions with tremendous current interest in fine chemical industries and synthetic organic chemistry: the hydrocyanation and hydroamination of alkynes. The hydrocyanation of unsaturated substrates is an important catalytic process in industry. The hydrocyanation of butadiene in the presence of nickel complexes, known as the DuPont ADN Process, is one of the most prominent examples of homogeneous catalysis on an industrial scale.[11] The catalyst system is based on in situ generation of a Ni(0) complex with a phosphite ligand; the industrial process started in 1970 with a monodentate phosphite,[12,13] which has changed to a bidentate ligand.[14] One major drawback of the Ni(0) catalysts arises from the formation of inactive nickel cyanides, in particular when the monodentate phosphite ligands dissociate and the catalyst is exposed to an excess of HCN. The reaction proceeds through the formation of relatively stable π-allylnickel cyanide intermediates, which participate in the successive carbon−carbon coupling.[12] On the other hand, the hydroamination of alkenes and alkynes, e.g., the direct amination of common unsaturated feedstocks, is a synthetically highly attractive transformation, for which still no general, efficient catalytic solution exists. Currently, catalysts effective for the hydroamination of activated olefins and alkynes are being developed.[15] Metal complexes of certain designs from across the periodic table involving lanthanides and early and late transition metals were found to catalyze the reaction. However, a general catalyst for the coupling of alkenes and alkynes to amines is still an unsolved problem.

In the present paper we report on the results of a theoretical analysis of the catalytic cycles of the hydrosilylation, hydrocyanation, and hydroamination of ethyne (acetylene) catalyzed by hydrido-bridged diplatinum complexes. Our purpose is to understand and advance the performance of the hydrido-bridged diplatinum catalysts in hydrosilylation, hydrocyanation, and hydroamination reactions by uncovering the elementary steps of the catalytic reactions and locating the intermediates and transition states involved in the catalytic cycle by monitoring the geometric and energetic reaction profile. To assess the efficiency of the catalytic cycles under turnover conditions, we used the energy span quantity, δE, which measures the energy difference between the summit and deepest species of the cycles. δE was recently[16] suggested to be a good indicator of the frequency of the catalytic cycle, that is, the turnover number (cycles per second).

Computational Details

In view of the good performance of density functional theory (DFT), we were compelled to perform DFT calculations at the B3LYP level of theory on all stationary points of the potential energy surfaces (PES) that we studied using the GAUSSIAN03

(11) Huthmacher, K.; Krill, S. In *Applied Homogeneous Catalysis with Organometallic Compounds*; Cornils, B., Hermann, W. A., Eds.; VCH: Weinheim, 1996; p 465.

(12) (a) Tolman, C. A.; McKinney, R. J.; Seidel, W. C.; Druliner, J. D.; Stevens, W. R. *Adv. Catal.* **1985**, *33*, 1. (b) Tolman, C. A. *J. Chem. Educ.* **1986**, *63*, 199.

(13) (a) Drinkard, W. C., Jr.; Kassal, R. J. U.S. Patent 3 496 217, 1970. (b) Drinkard, W. C. (DuPont) U.S. Patent 3 766 237, 1973. (c) Rapoport, M. (DuPont), U.S. Patent 4 371 474, 1983. (d) Tan, W. (DuPont) US Patent, 5 543 536, 1996.

(14) Coertz, W.; Keim, W.; Vogt, D.; Englert, U.; Boele, M. D. K.; van der Veen, L. A.; Kamer, P. C. J.; van Leeuwen, P. W. N. M. *J. Chem. Soc., Dalton Trans.* **1998**, 2981−2988, and references therein.

(15) For reviews of catalytic amine addition to C−C multiple bonds, see: (a) Odom, A. L. *Dalton Trans.* **2005**, 225−233. (b) Hultzsch, K. C. *Adv. Synth. Catal.* **2005**, *347*, 367−391. (c) Beller, M.; Seayad, J.; Tillack, A.; Jiao, H. *Angew. Chem., Int. Ed.* **2004**, *43*, 3368−3398. (d) Doye, S. *Synlett* **2004**, 1653−1672. (e) Hong, S.; Marks, T. J. *Acc. Chem. Res.* **2004**, *37*, 673−686. (f) Bytschkov, I.; Doye, S. *Eur. J. Org. Chem.* **2003**, *6*, 935−946. (g) Pohlki, F.; Doye, S. *Chem. Soc. Rev.* **2003**, *32*, 104−114. (h) Nobis, M.; Driessen-Holscher, B. *Angew. Chem., Int. Ed.* **2001**, *40*, 3983−3985. (i) Brunet, J. J.; Neibecker, D. In *Catalytic Heterofunctionalization from Hydroamination to Hydrozirconation*; Togni, A., Grützmacher, H., Eds.; Wiley-VCH: Weinheim, 2001; pp 91−141. (j) Müller, T. E.; Beller, M. *Chem. Rev.* **1998**, *98*, 675−703, and references therein. (k) Roundhill, D. M. *Catal. Today* **1997**, *37*, 155−165. (l) Hegedus, L. S. *Angew. Chem., Int. Ed. Engl.* **1988**, *27*, 1113−1126. (m) March, J. *Advanced Organic Chemistry*, 4th ed.; Wiley: New York, 1992; pp 768−770, and references therein. (n) Collman, J. P.; Hegedus, L. S.; Norton, J. R.; Finke, R. G. *Principles and Applications of Organotransition Metal Chemistry*; University Science Books: Mill Valley, CA, 1987; Chapters 7.4 and 17.1. (o) Bäckvall, J.-E. *Acc. Chem. Res.* **1983**, *16*, 335−342. (p) Trost, B. M.; Verhoeven, T. R. In *Comprehensive Organometallic Chemistry*; Wilkinson, G., Stone, F. G. A., Abel, E. W., Eds.; Pergamon Press: Oxford, U.K., 1982; Vol. 8, pp 892−895, and references therein.

(16) (a) Kozuch, S.; Amatore, C.; Jutand, A.; Shaik, S. *Organometallics* **2005**, *24*, 2319−2330. (b) Amatore, C.; Jutand, A. *J. Organomet. Chem.* **1999**, *576*, 254−278.

program suite.[17] The equilibrium and transition structures were fully optimized with Becke's three-parameter hybrid functional[18] combined with the Lee−Yang−Parr[19] correlation functional developed as the B3LYP method by Stephens et al.,[20] using the LANL2DZ basis set for the Pt atoms combined with the BS II of Frenking et al.,[21] which incorporates the Hay and Wadt[22] small-core relativistic effective core potential (ECP) with the optimized valence basis functions contracted to [441/2111/21] and the 6-31G(d,p) basis set for the rest of the nonmetal atoms. We will denote the computational approach used as B3LYP/LANL2DZ+BSII(Pt)∪6-31G**(L). The B3LYP method provides good descriptions of reaction profiles, including geometries, heats of reactions, and barrier heights.[23−25] In all computations no constraints were imposed on the geometry. Full geometry optimization was performed for each structure using Schlegel's analytical gradient method,[26] and the attainment of the energy minimum was verified by calculating the vibrational frequencies that result in the absence of imaginary eigenvalues. All stationary points have been identified for minimum (number of imaginary frequencies Nimag = 0) or transition states (Nimag = 1). The vibrational modes and the corresponding frequencies are based on a harmonic force field. This was achieved with the SCF convergence on the density matrix of at least 10^{-9} and a rms force less than 10^{-4} au. All bond lengths and bond angles were optimized to better than 0.001 Å and 0.1°, respectively. The computed electronic energies, the enthalpies of reactions, $\Delta_R H_{298}$, and the activation energies, $\Delta G^{\ddagger}_{298}$, were corrected to constant pressure and 298 K, for zero-point-energy (ZPE) differences and for the contributions of the translational, rotational, and vibrational partition functions. Furthermore, because the B3LYP approach underestimates activation barriers,[27] to obtain more reliable activation barriers, single-point energy calculations were also performed on the B3LYP/LANL2DZ+BSII(Pt)∪6-31G**(L) geometries at the higher CCSD(T) level of theory using the same basis set.[28] For transition state geometry determination, quasi-Newton transit-guided (QSTN) computations were performed.[29] Moreover, corrections of the transition states have been confirmed by intrinsic reaction coordinate (IRC) calculations, while intrinsic reaction paths (IRPs)[30] were traced from the various transition structures to make sure that no further intermediates exist.

Finally, because of the computational cost due to the relatively big size of the catalysts under consideration, to obtain a computationally convenient size, we used models resulting upon substitution of the alkyl groups of the phosphane ligand by H atoms. The use of such models does not alter the description of the "core" region of the compounds and is ultimately the most efficient and productive route to modeling the electronic structure and related properties of relatively big-sized transition metal coordination compounds.

Results and Discussion

Equilibrium Geometries and Electronic, Spectroscopic, and Bonding Properties of the Model "Precatalysts". The model hydrido-bridged diplatinum complexes [{Pt(L)(μ-H)-(PH_3)}$_2$] (L = SiH_3, CN, NH_2) used as catalysts in the hydrosilylation, hydrocyanation, and hydroamination reactions could result from the reaction of the zerovalent bis(ethylene)-(phosphane)platinum, [Pt$(C_2H_4)_2(PH_3)$], **1**, complex with H−SiH_3, H−CN, and H−NH_2, respectively. Selected geometric parameters for [{Pt(SiH_3)(μ-H)(PH_3)}$_2$], **2**, [{Pt(CN)(μ-H)(PH_3)}$_2$], **3**, and [{Pt(NH_2)(μ-H)(PH_3)}$_2$], **4**, model "precatalysts" computed at the B3LYP/LANL2DZ+BSII(Pt)∪6-31G**(L) level of theory are shown in Figure 1.

It can be seen that the diplatinum complexes **2**, **3**, and **4** are centrosymmetric (C_{2h} symmetry). Interestingly, complex **2** involves asymmetric Pt(μ-H)$_2$Pt bridges (the Pt−H and H···Pt bond distances differ by 30.1 pm), complex **3** involves almost symmetric Pt(μ-H)$_2$Pt bridges (the Pt−H and H···Pt bond distances differ by only 4.9 pm), while complex **4** involves perfectly symmetric Pt(μ-H)$_2$Pt bridges. Moreover, in the Pt(μ-H)$_2$Pt parallelogram the ∠H−Pt···H bond angles are 83.7°, 84.1°, and 84.0° in **2**, **3**, and **4**, respectively. Noteworthy is the perfect planarity of the (P)(Si)Pt−Pt(Si)(P) nuclear framework of the diplatinum complexes. The SiPtP angle of 90.7° in **2** is indicative of a square planar environment around each Pt center, which, however, is excessively distorted from the ideal square due to the hydride bridges formed. Such distortion is more pronounced in **3** and **4**, with the CPtP and NPtP angles being 84.2° and 73.5°, respectively. The Si···H separation distance of 274.8 pm in **2** is shorter than the sum of the van der Waals radii of the respective atoms (Si = 210 pm, H = 120 pm),[1] indicating that weak Si···H interactions still exist in the diplatinum complex, in line with experiment.[1a−c] Much weaker C···H interactions exist in complex **3**, with the C···H separation distance of 272.9 pm being also shorter than the sum of the van der Waals radii of the C and H atoms (C = 170 pm). However, in **4** there are no N···H interactions, as the N···H separation distance of 294.2 pm is longer than the sum of the van der Waals radii of the N and H atoms (N = 155 pm). It is clear that these multicenter interactions of the bridged hydride account well for the asymmetric Pt(μ-H)$_2$Pt bridges in **2** and **3**.

For the model complexes **2**, **3**, and **4** we identified in the regions of 1500−1700 and 1100 ± 300 cm^{-1} of the IR spectra the absorption bands related with the Pt(μ-H)$_2$Pt bridges. The vibrational modes along with the normal coordinate vectors (arrows) and the computed harmonic vibrational frequencies at the B3LYP/LANL2DZ+BSII(Pt)∪6-31G**(L) level of theory are depicted schematically in Figure 2.

It should be noted that in hydridometal complexes involving hydride bridges between two metal centers the hydrogen mode absorbs at low frequencies, ca. 1100 ± 300 cm^{-1}.[31] Noteworthy

(17) Frisch, M. J. T.; et al. *Gaussian 03*, Revision B.02; Gaussian, Inc.: Pittsburgh, PA, 2003. See Supporting Information for the remaining 80 authors.

(18) (a) Becke, A. D. *J. Chem. Phys.* **1992**, *96*, 2155−2160. (b) Becke, A. D. *J. Chem. Phys.* **1993**, *98*, 5648−5652.

(19) Lee, C.; Yang, W.; Parr, R. G. *Phys. Rev.* **1988**, *B37*, 785−789.

(20) (a) Stephens, P. J.; Devlin, F. J.; Chabalowski, C. F.; Frisch, M. J. *J. Phys. Chem.* **1994**, *98*, 11623. (b) Stephens, P. J.; Devlin, F. J.; Ashvar, C. S.; Bak, K. L.; Taylor, P. R.; Frisch, M. J. *ACS Symp. Ser.* **1996**, *629*, 105.

(21) Frenking, G.; Antes, I.; Böhme, M.; Dapprich, S.; Ehlers, A. W.; Jonas, V.; Neuhaus, A.; Otto, M.; Stegmann, R.; Veldkamp, A.; Vyboishchikov, S. F. In *Reviews in Computational Chemistry*; Lipkowitz, K. B., Boyds, D. B., Eds.; VCH: New York, 1996; Vol. 8, p 63.

(22) (a) Hay, P. J.; Wadt, W. R. *J. Chem. Phys.* **1985**, *82*, 270−283. (b) Wadt, W. R.; Hay, P. J. *J. Chem. Phys.* **1985**, *82*, 284−298. (c) Hay, P. J.; Wadt, W. R. *J. Chem. Phys.* **1985**, *82*, 299−310.

(23) Vosko, S. H.; Wilk, L.; Nusair, M. *Can. J. Phys.* **1980**, *58*, 1200−1211.

(24) Baker, J.; Muir, M.; Andzelm, J.; Scheiner, A. In *Chemical Applications of Density-Functional Theory*; Laird, B. B., Ross, R. B., Ziegler, T., Eds.; ACS Symposium Series 629; American Chemical Society: Washington, DC, 1996.

(25) Curtiss, L. A.; Raghavachari, K.; Redfern, P. C.; Pople, J. A. *J. Chem. Phys.* **1997**, *106*, 1063.

(26) Schlegel, H. B. *J. Comput. Chem.* **1982**, *3*, 214−218.

(27) (a) Lynch, B. J.; Fast, P. L.; Harris, M.; Truhlar, D. G. *J. Phys. Chem. A* **2000**, *104*, 4811−4815. (b) Lynch, B. J.; Truhlar, D. G. *J. Phys. Chem. A* **2001**, *105*, 2936−2941. (c) Poater, J.; Sola, M.; Duran, M.; Robles, L. *Phys. Chem. Chem. Phys.* **2002**, *4*, 722−731.

(28) Pople, J. A.; Head-Gordon, M.; Raghavachari, K. *J. Chem. Phys.* **1987**, *87*, 5968−5975.

(29) Head-Gordon, M. P.; Frisch, M. J. *Chem. Phys. Lett.* **1988**, *153*, 503−506.

(30) (a) Gonzalez, C.; Schlegel, H. B. *J. Chem. Phys.* **1989**, *90*, 2154−2161. (b) Gonzalez, C.; Schlegel, H. B. *J. Phys. Chem.* **1990**, *94*, 5523−5527.

(31) Kaesz, H. D.; Sailant, R. B. *Chem. Rev.* **1972**, *72*, 231−281.

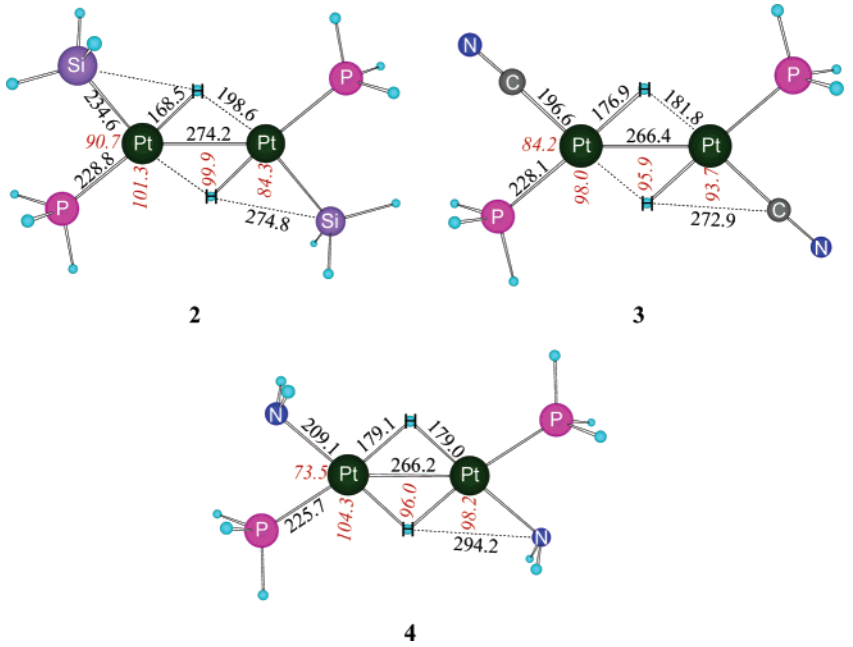

Figure 1. Equilibrium geometries (bond lengths in pm, angles in deg) of the model [{Pt(SiH_3)(μ-H)(PH_3)}$_2$], **2**, [{Pt(CN)(μ-H)(PH_3)}$_2$], **3**, and [{Pt(NH_2)(μ-H)(PH_3)}$_2$], **4** "precatalysts", computed at the B3LYP/LANL2DZ+BSII(Pt)∪6-31G**(L) level of theory.

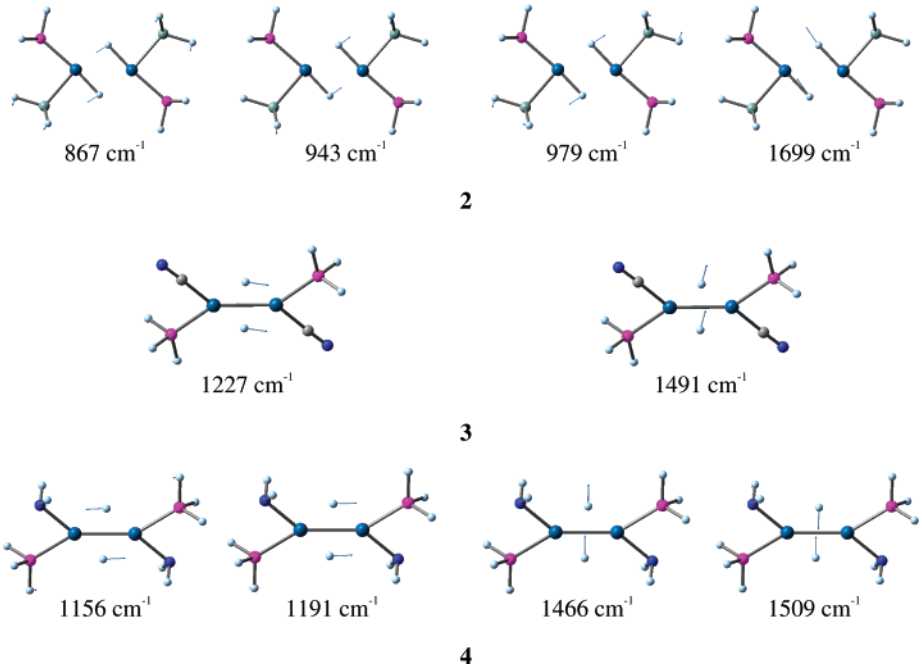

Figure 2. Vibrational modes along with the normal coordinate vectors (arrows) and the unscaled harmonic vibrational frequencies related to the Pt(μ-H)$_2$Pt moiety of the model [{Pt(SiH_3)(μ-H)(PH_3)}$_2$], **2**, [{Pt(CN)(μ-H)(PH_3)}$_2$], **3**, and [{Pt(NH_2)(μ-H)(PH_3)}$_2$], **4**, "precatalysts".

is the different hydride vibrational mode in **3** and **4** relative to that of **2** (Figure 2), which is reflected in the computed lower harmonic vibrational frequencies. This is consistent with the longer Pt−H bond lengths and the more symmetric Pt(μ-H)$_2$Pt bridges in **3** and **4** than in **2**.

The hydrido-bridged diplatinum complexes **2**, **3**, and **4** obeying the framework electron count (FEC) rule introduced by Alvarez et al.[32] (FEC = 8) are expected to involve weak intermetallic Pt···Pt interactions. Such intermetallic interactions are mirrored in the computed Pt···Pt separation distances of 274.2, 266.4, and 266.2 pm in **2**, **3**, and **4**, respectively, which are very close to the sum (262 pm) of the covalent radii. To assess the strength of the Pt···Pt interactions, we computed the dissociation energies of the dimers to yield the monomeric species [Pt(SiH_3)(H)(PH_3)], **5**, [Pt(CN)(H)(PH_3)], **6** (figures in italics), and [Pt(NH_2)(H)(PH_3)], **7**. The predicted dissociation energies were found to be 25.4, 49.4, and 47.3 kcal/mol for **2**, **3**, and **4**, respectively, in terms of ΔE_0 at the B3LYP/LANL2DZ+BSII(Pt)∪6-31G**(L) level of theory. The computed dissociation energy is the sum of the energy due to the two hydrogen bonds between the Pt centers and the energy due to the intermetallic Pt···Pt interactions. The higher dissociation energies in **3** and **4** are indicative of the stronger intermetallic Pt···Pt interactions than in **2**. The existence of the intermetallic Pt···Pt interactions is also substantiated by the respective

(32) Alvarez, S.; Palacios, A. A.; Aullon, G. *Coord. Chem. Rev.* **1999**, *185−186*, 431, and references therein.

Scheme 2. σ-, π-, and δ-Type MOs Describing the Intermetallic Pt···Pt Interactions in the Hydrido-Bridged Diplatinum Complexes 2, 3, and 4

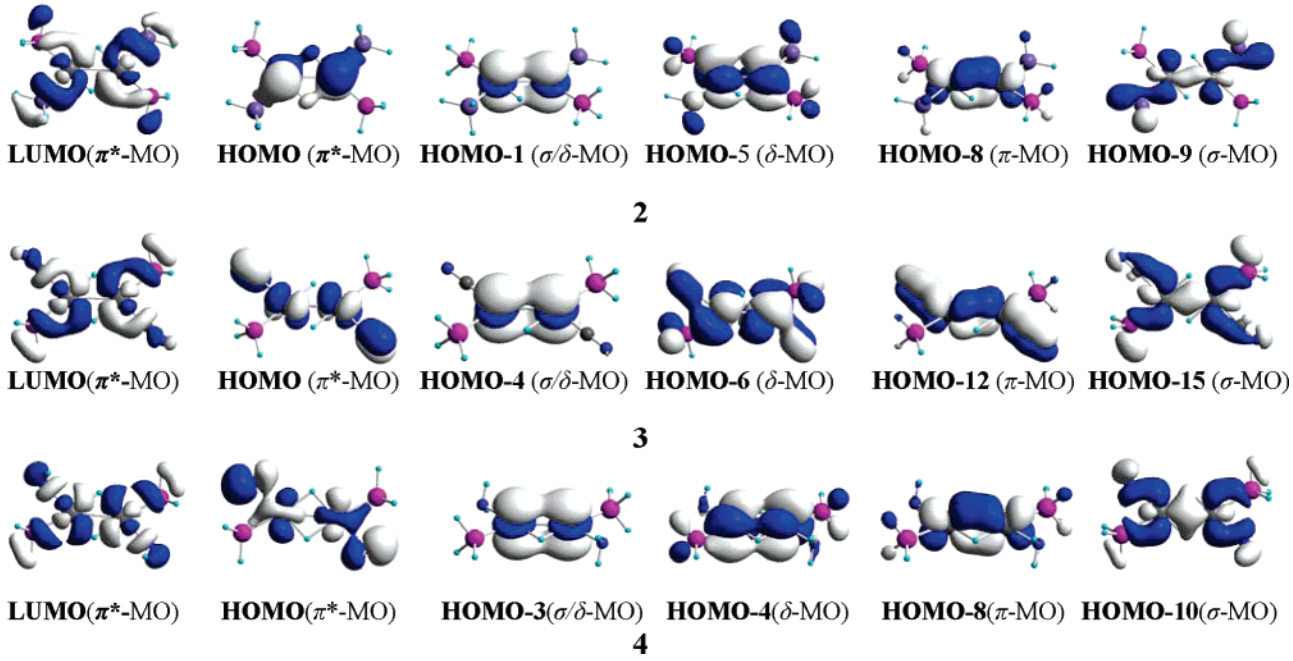

molecular orbital interactions (Scheme 2), which correspond to σ-, π-, and δ-type bonding interactions.

Equilibrium Geometries and Electronic, Spectroscopic, and Bonding Properties of the Model "Catalysts". Considering that the first step of the hydrosilylation, hydrocyanation, and hydroamination reactions involves the cleavage of the hydrido-bridges in the diplatinum complexes promoted by the incoming alkyne substrate, it is important to study first the coordinatively unsaturated 14e mononuclear Pt(II) species consisting of the catalytically "active" species in the catalytic cycle.

Selected geometric and spectroscopic parameters for the model [PtH(L)(PH_3)] (L = SiH_3, **5**, CN, **6**, NH_2, **7**) "catalysts" computed at the B3LYP/LANL2DZ+BSII(Pt)∪6-31G**(L) level of theory are summarized in Figure 3.

It can be seen that all monomeric species adopt a planar T-shaped structure with the terminal hydride in *trans* position to the phosphane ligand; the ∠P−Pt−H bond angles are almost 180.0°. The Pt−H bond length in **5** is slightly longer than in **6** and **7**. This could be due to the weak Si···H interactions, as the Si···H separation distance of 239.8 pm is much shorter than the sum of the van der Waals radii of the respective atoms. This is reflected in the smaller SiPtH bond angle of 73.6° in **5** and is further substantiated by the computed Mulliken bond overlap population (e.g., the electron population in the overlap region of the atomic orbitals of the interacting atoms) of 0.028.

In the IR spectra of **5**, **6**, and **7** the strong Pt−H stretching vibrational bands occur at 2130.8, 2218.5, and 2175.5 cm^{-1}, respectively, as expected for platinum complexes involving terminal hydride ligands,[1b] and are consistent with the Pt−H bond length.

According to the NBO analysis, the σ(Pt−H) natural orbitals describing the terminal Pt−H bond in the hydride platinum complexes **5**, **6**, and **7** are constructed from $sd^{1.43}$, $sd^{1.00}$, and $sd^{0.75}$ hybrids on the platinum atom, interacting in-phase with the 1s orbital on the terminal hydride, thus having the forms $\sigma(Pt-H) = 0.7117h_{Pt} + 0.7025s_H$, $\sigma(Pt-H) = 0.7187h_{Pt} + 0.6953s_H$, and $\sigma(Pt-H) = 0.6786h_{Pt} + 0.7343s_H$, respectively. Noteworthy is the decrease of the d character in the sd hybrids going from **5** to **7** and the concomitant increase of the contribution of the 1s AO of the hydride ligand to the bonding σ(Pt−H) MO. It should also be noticed that the LUMO of complexes **5**, **6**, and **7** corresponds to a dsp^2-hybridized orbital directed toward the open coordination site of a square planar coordination environment, thereby being capable of interacting with the HOMO of any nucleophile, such as ethene, ethyne, isonitrile, and phosphane ligands, to afford the more stable 16*e* square planar complexes.

Let us now go deeper into the details of the hydrosilylation, hydrocyanation, and hydroamination of ethyne catalyzed by the model "catalysts" **5**, **6**, and **7**, respectively.

Catalytic Cycle of the Hydrosilylation of Ethyne Catalyzed by the Model "Catalyst" 5. The predicted catalytic cycle for the hydrosilylation of ethyne using model "catalyst" **5** is depicted schematically in Figure 4. The equilibrium structures of the relevant stationary points in the PES of the catalytic cycle

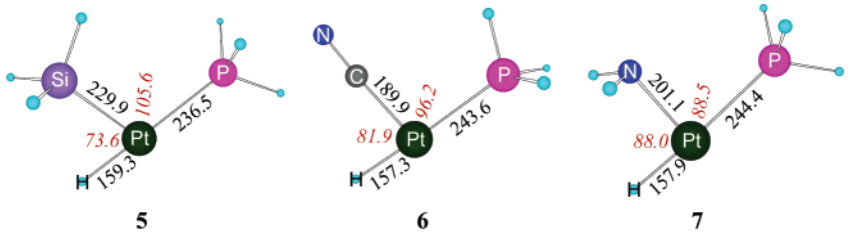

5 **6** **7**

Figure 3. Equilibrium geometries (bond lengths in pm, angles in deg) of the model [Pt(SiH_3)(H)(PH_3)], **5**, [Pt(CN)(H)(PH_3)], **6**, and [Pt(NH_2)(H)(PH_3)], **7**, "catalysts", computed at the B3LYP/LANL2DZ+BSII(Pt)∪6-31G**(L) level of theory.

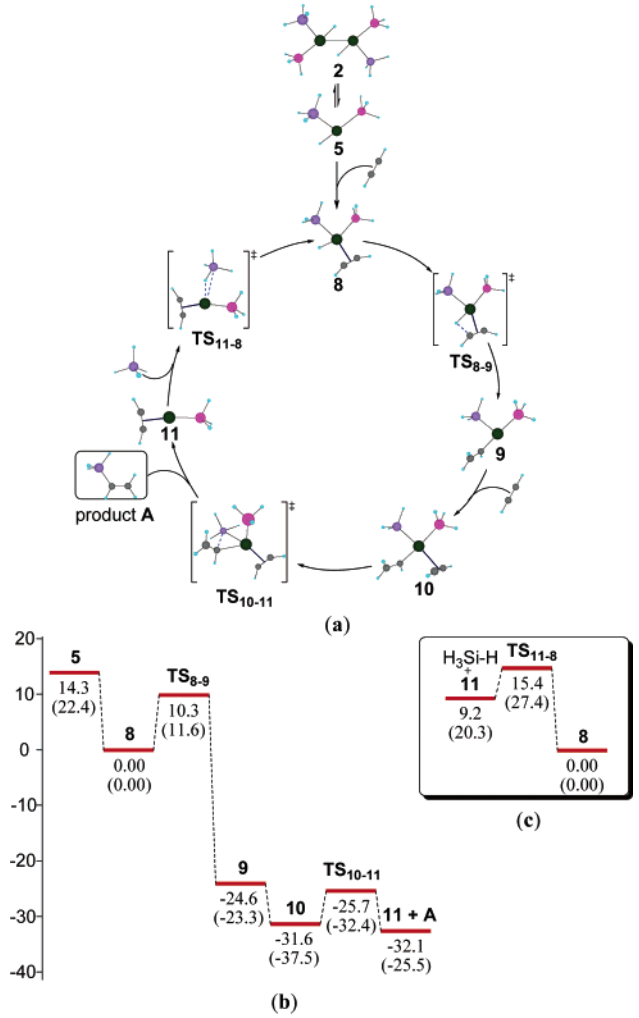

Figure 4. (a) Catalytic cycle for the hydrosilylation of ethyne catalyzed by the model "catalyst" [Pt(SiH_3)(H)(PH_3)], **5**; (b) reaction energy profile (ΔE_0 in kcal/mol) of the catalytic cycle computed at the B3LYP/LANL2DZ+BSII(Pt)∪6-31G**(L) and CCSD(T)/LANL2DZ+BSII(Pt)∪6-31G**(L)//B3LYP/LANL2DZ+BSII(Pt)∪6-31G**(L) (figures in parentheses) levels of theory; (c) the oxidative addition reaction energy profile that regenerates the catalytic species **8**.

computed at the B3LYP/LANL2DZ+BSII(Pt)∪6-31G**(L) level of theory are shown in Figures 5, while the relative energies, heats of reactions, and activation barriers are summarized in Table 1.

Attachment of the ethyne to mononuclear species **5** leads to the lengthening of the Pt−H and Pt−Si bonds by 0.6 and 8.5 pm, respectively, while the Pt−P bond is shortened by 1.9 pm. These structural changes are reflected in the respective vibrational frequencies; the stretching vibrations of the Pt−H, Pt−Si, and Pt−P bonds are predicted to be 2119, 341, and 293 cm^{-1}, respectively. It should be noticed that the coordination of the ethyne molecule to the platinum center results in the lengthening of the C≡C triple bond by 3.9 pm, with a ν(C≡C) stretching vibrational frequency of 1873 cm^{-1}. Noteworthy is the deviation from linearity of the coordinated ethyne molecule; the bending H−C≡C angle was found to be 158.6°. Moreover, upon coordination of the ethyne molecule with the catalyst **5**, the P−Pt−H bond angle changes from 179.2° to 157.3°.

A π-ethyne adduct of the "catalytically" active monomeric species, with the ethyne ligand on the coordination plane occupying a *trans* position to the silyl group, has been successfully located as distinct intermediate **8**, in the first stage of the catalytic cycle. The formation of intermediate **8** was calculated to be exoergic by −14.3 (−22.4) kcal/mol at the B3LYP (CCSD(T)) levels of theory. Including entropic effects (ΔG) reduces the exergonicity to −3.2 kcal/mol.

According to the NBO analysis, the σ(Pt−H) natural orbital is constructed from an $sd^{1.13}$ hybrid (52.87% d character) on the platinum atom, $h_{Pt} = -0.684(6s)_{Pt} + 0.705(5d_{x^2-y^2})_{Pt} + 0.155(5d_{z^2})_{Pt}$, interacting in-phase with the 1s orbital on the terminal hydride, thus having the form $\sigma(Pt-H) = 0.713h_{Pt} + 0.701s_H$. The terminal hydride ligand acquires a negative natural charge of −0.10 |e|.

The next step of the catalytic cycle involves a one-step migratory insertion of ethyne into the Pt−H bond through **TS_{8-9}**, yielding intermediate **9** with an activation barrier of 10.8 (11.6) kcal/mol in terms of $\Delta G^{\ddagger}(\Delta E_{CCSD(T)}{}^{\ddagger})$. The relatively low activation barrier illustrates that the hydride migration to the coordinated ethyne proceeds without the eventual coordination of a second ethyne molecule to the 16*e* square planar complex. The transition state **TS_{8-9}** exhibits some interesting structural features (Figure 5). The distance between the migrating hydride ligand and the nearest acceptor C atom of the ethyne ligand has dramatically shortened by 90.3 pm with respect to the corresponding distance in complex **8**. The Pt−C(centroid) distance in **TS_{8-9}** is shortened by 4.8 pm, while the C−C bond distance of the coordinated ethyne molecule is further lengthened by 3.0 pm with respect to species **8**. In the vibrational mode corresponding to the imaginary frequency of **TS_{8-9}**, $\nu_i = 784$ cm^{-1}, the dominant motions involve the transferring hydride along with the nearest acetylenic H atom of the coordinated H−C≡C−H molecule.

The intermediate **9**, being 24.6 (23.3) kcal/mol in terms of ΔE_0 more stable than intermediate **8** at the B3LYP (CCSD(T)) levels, is a coordinatively unsaturated 14*e* Pt(II) complex with a T-shaped structure ($\angle$C−Pt−P = 176.3°), involving a coordinated ethenyl group in a perpendicular orientation with respect to the coordination plane. The coordinatively unsaturated 14*e* Pt(II) complex **9** captures immediately a second molecule

Table 1. Relative Energies, Enthalpies, Gibbs Free Energies, and Activation Barriers (kcal/mol) of the Hydrosilylation of Ethyne Catalyzed by Model "Catalyst" 5 Computed at the B3LYP/LANL2DZ+BSII(Pt)∪6-31G(L) and CCSD(T)/LANL2DZ+BSII(Pt)∪6-31G**(L)//B3LYP/LANL2DZ+BSII(Pt)∪6-31G**(L) Levels of Theory**

	ΔE_0	ΔH	ΔG	$\Delta E_{CCSD(T)}$	$\Delta E_0{}^{\ddagger}$ ($\Delta H^{\ddagger}$) [$\Delta G^{\ddagger}$]	$\Delta E_{CCSD(T)}{}^{\ddagger}$
			Hydrosilylation			
5 + ethyne	14.3	14.9	3.2	22.4		
8	0.0	0.0	0.0	0.0		
TS_8−9	10.3	9.8	10.8	11.6	10.3 (9.8) [10.8]	11.6
9	−24.6	−24.8	−25.0	−23.3		
10	−31.6	−31.9	−23.1	−37.5		
TS_{10}−11	−25.7	−27.2	−15.2	−32.4	5.9 (4.7) [7.9]	5.1
11 + product **A**	−32.1	−33.1	−34.5	−25.5		
11 + hydrosilane	9.2	9.6	−11.6	20.3		
TS_{11}−8	15.4	15.7	−5.7	27.4	6.2 (6.1) [5.9]	7.1

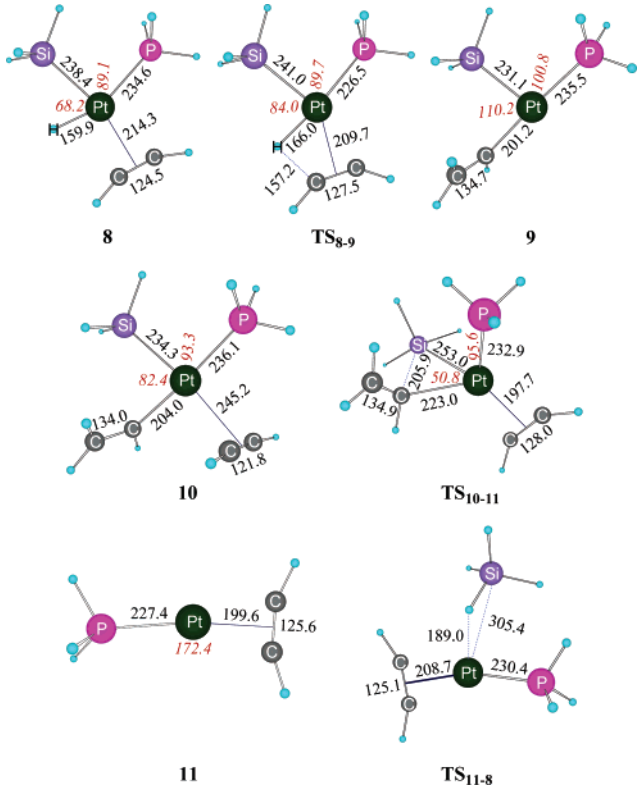

Figure 5. Equilibrium structures (bond lengths in pm, angles in deg) of the relevant stationary points in the PES of the catalytic cycle for the hydrosilylation of ethyne using model catalyst **5**, computed at the B3LYP/LANL2DZ+BSII(Pt)∪6-31G**(L) level of theory.

of the ethyne substrate, forming intermediate **10**, which through a reductive elimination process affords the product **A** ($H_2C{=}CHSiH_3$) and the catalytic species **11**. The latter, upon oxidative addition with hydrosilane, regenerates the catalytic species **8**, thus completing the catalytic cycle. During the course of the reductive elimination process the silyl ligand is transferred to the acceptor C atom of the coordinated ethenyl group via the transition state $\mathbf{TS_{10-11}}$, surmounting a relatively low energy barrier of 5.9 (5.1) kcal/mol. Moreover, the reductive elimination corresponds to an almost thermoneutral process at the B3LYP level ($\Delta E_0 = -0.5$ kcal/mol), but it is slightly endoergic at the CCSD(T) level ($\Delta E_0 = 12.0$ kcal/mol). In $\mathbf{TS_{10-11}}$ the silyl group was inclined toward the ethenyl group by 39.2° (Si−Pt−C = 50.8°). The distance between the migrating silyl ligand and the nearest C atom of the acceptor ethenyl group is 18.6 pm longer than the C−Si bond length in the final product **A**, whereas the C−C bond distance is only 0.9 pm longer than the respective C−C bond length of product **A**. This means that $\mathbf{TS_{10-11}}$ is a late transition state. In the vibrational mode corresponding to the imaginary frequency of $\mathbf{TS_{10-11}}$, $\nu_i = 162$ cm^{-1}, the dominant motions involve the transferring silyl group along with the nearest C atom of the $H_2C{=}CH-$ ligand.

The oxidative addition of hydrosilane to the coordinatively unsaturated 14*e* Pt(0) complex **11** regenerating the "true" catalytic species **8** and closing the catalytic cycle corresponds to an exothermic process, with exothermicity of −9.2 (−20.3) kcal/mol at the B3LYP (CCSD(T)) levels, and surmounts a relatively low activation barrier of 5.9 (7.1) kcal/mol in terms of $\Delta G^{\ddagger}(\Delta E_{CCSD(T)}{}^{\ddagger})$. The transition state $\mathbf{TS_{11-8}}$ involves a loosely associated silane molecule interacting with the Pt(0) metal center in a κ^2-Si,H bonding mode. In the vibrational mode corresponding to the imaginary frequency of $\mathbf{TS_{10-8}}$, $\nu_i = 83$ cm^{-1}, the dominant motion involves the stretching of the coordinated Si−H bond.

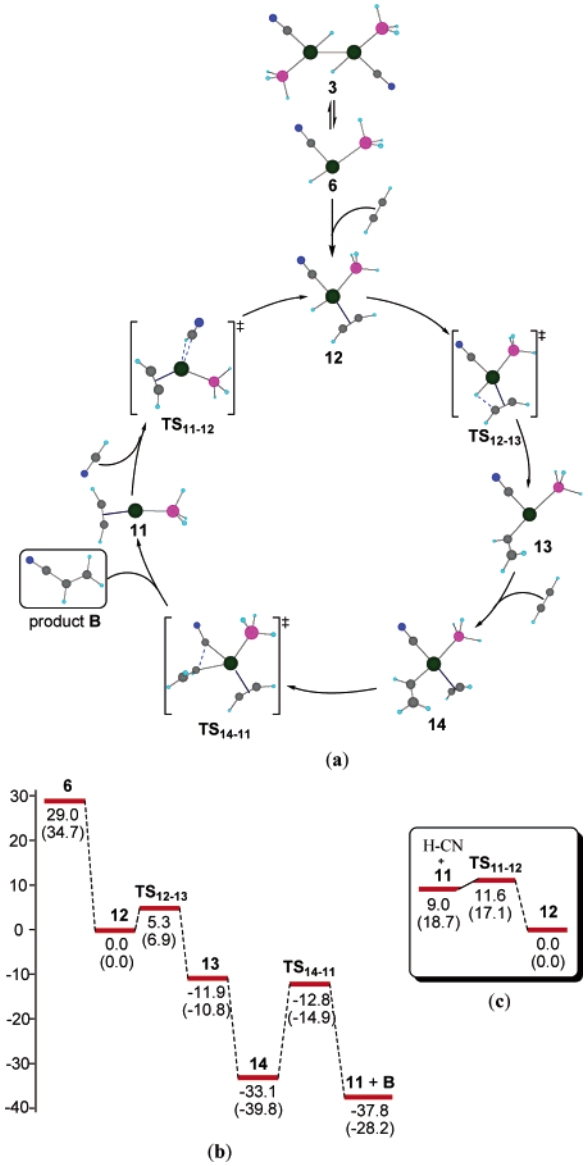

Figure 6. (a) Catalytic cycle for the hydrocyanation of ethyne catalyzed by the model "catalyst" [Pt(CN)(H)(PH_3)], **6**; (b) reaction energy profile (ΔE_0 in kcal/mol) of the catalytic cycle computed at the B3LYP/LANL2DZ+BSII(Pt)∪6-31G**(L) and CCSD(T)/LANL2DZ+BSII(Pt)∪6-31G**(L)//B3LYP/LANL2DZ+BSII(Pt)∪6-31G**(L) (figures in parentheses) levels of theory; (c) the oxidative addition reaction energy profile that regenerates the catalytic species **12**.

In summary the rate-limiting step for the hydrosilylation of ethyne catalyzed by the diplatinum complexes is predicted to be the step of the hydride migration to the acceptor C atom of the coordinated ethyne substrate. Moreover the efficiency of the catalytic cycle of the hydrosilylation process is quantified by the energy span quantity, δE, of 47.5 (52.9) kcal/mol at the B3LYP (CCSD(T)) levels.

Catalytic Cycle of the Hydrocyanation of Ethyne Catalyzed by the Model "Catalyst" 6. The predicted catalytic cycle for the hydrocyanation of ethyne using model "catalyst" **6** is depicted schematically in Figure 6. The equilibrium structures of the relevant stationary points in the PES of the catalytic cycle computed at the B3LYP/LANL2DZ+BSII(Pt)∪6-31G**(L) level of theory are shown in Figures 7, while the relative

Table 2. Relative Energies, Enthalpies, Gibbs Free Energies, and Activation Barriers (kcal/mol) of the Hydrocyanation of Ethyne Catalyzed by Model "Catalyst" 6 Computed at the B3LYP/LANL2DZ+BSII(Pt)∪6-31G(L) and CCSD(T)/LANL2DZ+BSII(Pt)∪6-31G**(L)//B3LYP/LANL2DZ+BSII(Pt)∪6-31G**(L) Levels of Theory**

	ΔE_0	ΔH	ΔG	$\Delta E_{CCSD(T)}$	$\Delta E_0^{\ddagger}$ ($\Delta H^{\ddagger}$) [$\Delta G^{\ddagger}$]	$\Delta E_{CCSD(T)}^{\ddagger}$
			Hydrocyanation			
6 + ethyne	29.0	29.6	18.2	34.7		
12	0.00	0.00	0.00	0.00		
TS$_{12}$−13	5.3	5.0	5.8	6.9	5.3 (5.0) [5.8]	6.9
13	−11.9	−11.8	−12.8	−10.8		
14	−33.1	−33.5	−23.9	−39.8		
TS$_{14}$−11	−12.8	−13.8	−3.0	−14.9	20.3 (19.7) [20.9]	24.9
11 + product **B**	−37.8	−38.6	−40.1	−28.2		
11 + hydrocyano	9.0	9.6	−1.1	18.7		
TS$_{11}$−12	11.6	11.5	11.2	20.3	2.6 (1.9) [12.3]	1.6

energies, heats of reactions, and activation barriers are summarized in Table 2.

The first stage of the catalytic cycle involves the coordination of the ethyne molecule with the "catalytically" active Pt(II) monomeric species, yielding the π-ethyne adduct (intermediate **12**). In this adduct the ethyne molecule occupies a *trans* position to the CN ligand with a coplanar orientation with respect to the coordination plane of the Pt(II) complex. The formation of intermediate **12** was calculated to be exoergic by −29.0 (−34.7) kcal/mol at the B3LYP (CCSD(T)) levels of theory. The inclusion of entropic effects (ΔG) reduces the exothermicity to −18.2 kcal/mol. It should be noted that the first step of the hydrocyanation process is more exoergic than the corresponding step of the hydrosilylation process by 14.7 (12.3) kcal/mol at the B3LYP (CCSD(T)) levels of theory.

Attachment of the ethyne to catalytic species **6** leads to the lengthening of the Pt−H, Pt−CN, and Pt−P bonds by 0.7, 8.1, and 2.6 pm, respectively. These structural changes are reflected in the respective vibrational frequencies; the stretching vibrations of the Pt−H, Pt−C, and Pt−P bonds are predicted to be 2203, 465, and 261 cm^{-1}, respectively. Upon coordination of the ethyne molecule to the platinum center, the C≡C triple bond is lengthened by 3.8 pm, while the H−C≡C moiety is bent away from the Pt(II) center with the bending angle being 157.6°. Moreover, in the intermediate **12** the P−Pt−H bond angle deviates from linearity by 16.6°. The unscaled ν(C≡C) and ν(C≡N) stretching vibrational frequencies are predicted to be 1882 and 2265 cm^{-1}, respectively. The vibrational modes characterizing the coordination of the ethyne molecule with the Pt(II) metal center are the ν(Pt−C$_2$(centroid)) and ν_{as}(Pt−C$_2$) stretching vibrational modes that absorb at 331 and 421 cm^{-1}, respectively.

The σ(Pt−H) natural orbital is constructed from an sd hybrid (49.94% d character) on the platinum atom, $h_{Pt} = -0.706(6s)_{Pt} - 0.456\ (5d_{xy})_{Pt} + 527(5d_{x^2-y^2})_{Pt} + 0.111(5d_{z^2})_{Pt}$, interacting in-phase with the 1s orbital on the bridging hydride, thus having the form $\sigma(Pt-H) = 0.728h_{Pt} + 0.686s_H$. The Pt(II) metal center acquires a positive natural charge of 0.30 $|e|$, while the terminal hydride ligand acquires a negative natural charge of −0.04 $|e|$.

The next step of the catalytic cycle involves the migratory insertion of ethyne into the Pt−H bond through **TS$_{12-13}$**, yielding intermediate **13**, with an activation barrier of 5.8 (6.9) kcal/mol in terms of $\Delta G^{\ddagger}$($\Delta E_{CCSD(T)}^{\ddagger}$). The activation barrier is lower than the corresponding activation barrier of the hydrosilylation process. The structural features of the transition state **TS$_{12-13}$** are similar to those of **TS$_{8-9}$**. The distance between the migrating hydride ligand and the nearest acceptor C atom of the ethyne ligand has dramatically shortened by 67.3 pm with respect to the corresponding distance in complex **12**. The Pt−C(centroid) distance in **TS$_{12-13}$** is shortened by 4.0 pm, while

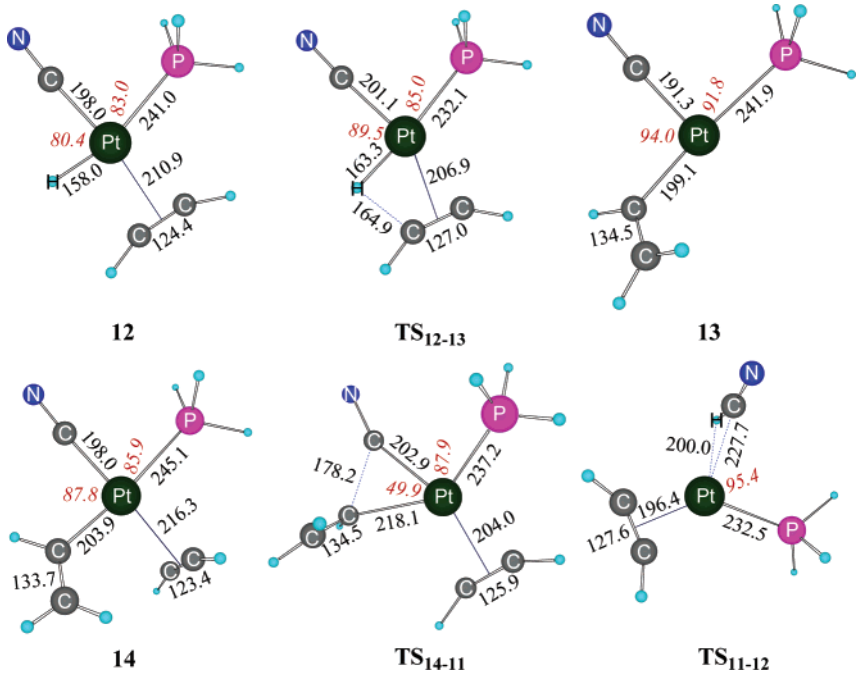

Figure 7. Equilibrium structures (bond lengths in pm, angles in deg) of the relevant stationary points in the PES of the catalytic cycle for the hydrocyanation of ethyne using model catalyst **6**, computed at the B3LYP/LANL2DZ+BSII(Pt)∪6-31G**(L) level of theory.

the C−C bond distance of the coordinated ethyne molecule is further lengthened by 2.6 pm with respect to intermediate **12**. In the vibrational mode corresponding to the imaginary frequency of $\mathbf{TS_{12-13}}$, ν_i = 678 cm^{-1}, the dominant motions involve the transferring hydride along with the nearest acetylenic H atom of the coordinated H−C≡C−H molecule. The lower imaginary frequency of $\mathbf{TS_{12-13}}$ with respect to that of $\mathbf{TS_{8-9}}$ is consistent with the lower activation barrier for the transformation **12** → **13** than the transformation **8** → **9**. The intermediate **13**, being 11.9 (10.8) kcal/mol in terms of ΔE_0 more stable than intermediate **12** at the B3LYP (CCSD(T)) levels, is a coordinatively unsaturated 14*e* Pt(II) complex with a T-shaped structure (∠C−Pt−P = 174.1°), involving a coordinated ethenyl group in a nearly perpendicular orientation with respect to the coordination plane.

The subsequent step of the catalytic cycle involves coordination of a second ethyne molecule to the Pt(II) center of intermediate **13**, yielding the coordinatively unsaturated 16*e* Pt(II) complex **14**, which via a reductive elimination process affords the product **B** (H_2C═CHCN) and the catalytic species **11**. Then, oxidative addition of H−CN to intermediate **11** regenerates the catalytic species **12**, closing thus the catalytic cycle. During the course of the reductive elimination process the cyanide ligand is transferred to the acceptor C atom of the coordinated ethenyl group via the transition state $\mathbf{TS_{14-11}}$, surmounting an energy barrier of 20.9 (24.9) kcal/mol at the B3LYP (CCSD(T)) levels. Notice that the cyanide migration demands a much higher activation barrier than the migration of the silyl group. It is evident that the reductive elimination step is the rate-limiting step for the hydrocyanation process. As in the case of hydrosilylation, the reductive elimination step of hydrocyanation corresponds to a slightly exothermic process at the B3LYP level (ΔE_0 = −4.7 kcal/mol), but it is endoergic at the CCSD(T) level (ΔE_0 = 11.6 kcal/mol). In $\mathbf{TS_{14-11}}$ the cyanide ligand was inclined toward the ethenyl group by 40.1° (C−Pt−C = 49.9°). The distance between the migrating cyanide ligand and the nearest C atom of the acceptor ethenyl group is 35.0 pm longer than the C−CN bond length in the final product **B**, whereas the C−C bond distance is only 0.6 pm shorter than the respective C−C bond length of product **B**. In the vibrational mode corresponding to the imaginary frequency of $\mathbf{TS_{14-11}}$, ν_i = 386 cm^{-1}, the dominant motions involve the transferring cyanide group along with the nearest C atom of the H_2C═CH− ligand.

The oxidative addition of H−CN to the coordinatively unsaturated 14*e* Pt(0) complex **11** regenerating the "true" catalytic species **12** corresponds to an exothermic process, with exothermicity of −9.0 (−18.7) kcal/mol at the B3LYP (CCSD(T)) levels, and surmounts a low activation barrier of 11.6 (17.1) kcal/mol in terms of $\Delta G^{\ddagger}$($\Delta E_{CCSD(T)}^{\ddagger}$). These activation barriers are slightly higher than the corresponding barriers of the hydrosilylation process. The transition state $\mathbf{TS_{11-12}}$ involves a loosely associated H−CN molecule interacting with the Pt(0) metal center in a κ^2-C,H bonding mode. In the vibrational mode corresponding to the imaginary frequency of $\mathbf{TS_{10-12}}$, ν_i = 67 cm^{-1}, the dominant motion involves the stretching of the coordinated C−H bond.

In summary the geometric and energetic profile of the hydrocyanation of ethyne catalyzed by the hydrido-bridged diplatinum complexes closely resembles that of the respective hydrosilylation reaction, and therefore the hydrido-bridged diplatinum complexes are expected to exhibit a catalytic activity in hydrocyanation comparable to that of hydrosilylation. This is substantiated by the computed values of the energetic span

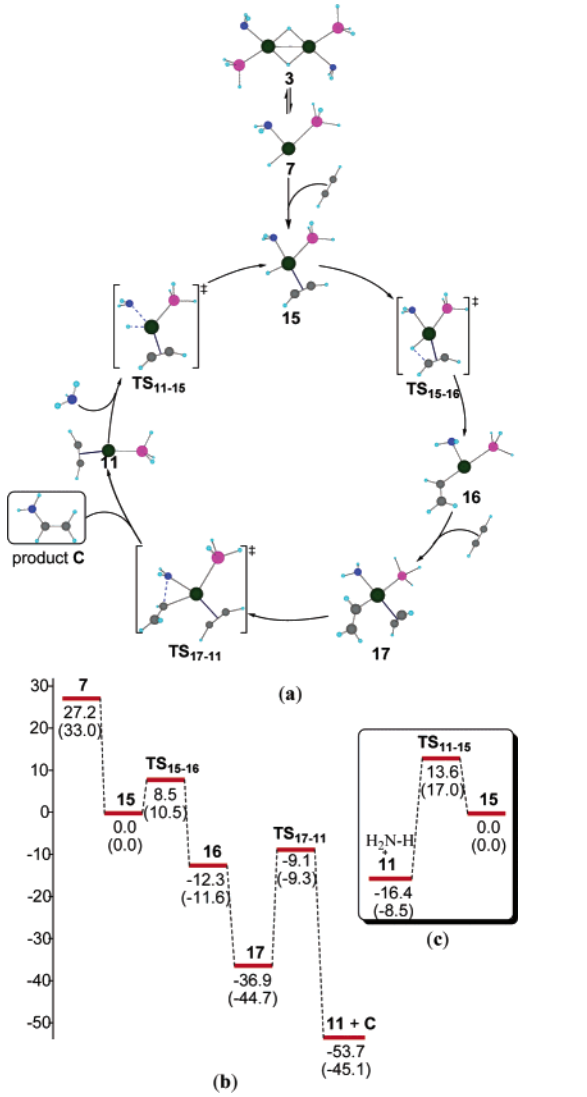

Figure 8. (a) Catalytic cycle for the hydroamination of ethyne catalyzed by the model "catalyst" [Pt(NH_2)(H)(PH_3)], **7**; (b) reaction energy profile (ΔE_0 in kcal/mol) of the catalytic cycle computed at the B3LYP/LANL2DZ+BSII(Pt)∪6-31G**(L) and CCSD(T)/LANL2DZ+BSII(Pt)∪6-31G**(L)//B3LYP/LANL2DZ+BSII(Pt)∪6-31G**(L) (figures in parentheses) levels of theory; (c) the oxidative addition reaction energy profile that regenerates the catalytic species **15**.

of the cycles, δE, which for hydrocyanation were found to be 49.4 (45.3) kcal/mol at the B3LYP (CCSD(T)) levels. Moreover, the Pt(II) catalytic species are expected to be superior catalysts to the tetrahedrally coordinated zerovalent nickel catalysts used in hydrocyanation of unsaturated substrates,[12−14,33] since they have easily accessible open coordination sites capable of accommodating the unsaturated substrates.

Catalytic Cycle of the Hydroamination of Ethyne Catalyzed by the Model "Catalyst" 7. The catalytic cycle for the hydroamination of ethyne using model "catalyst" **7** is depicted schematically in Figure 8. The equilibrium structures of the relevant stationary points in the PES of the catalytic cycle computed at the B3LYP/LANL2DZ+BSII(Pt)∪6-31G**(L) level of theory are shown in Figures 9, while the relative energies, heats of reactions, and activation barriers are summarized in Table 3.

(33) Burello, E.; Marion, P.; Galland, J.-C.; Chamard, A. *Adv. Synth. Catal.* **2005**, *347*, 803−810.

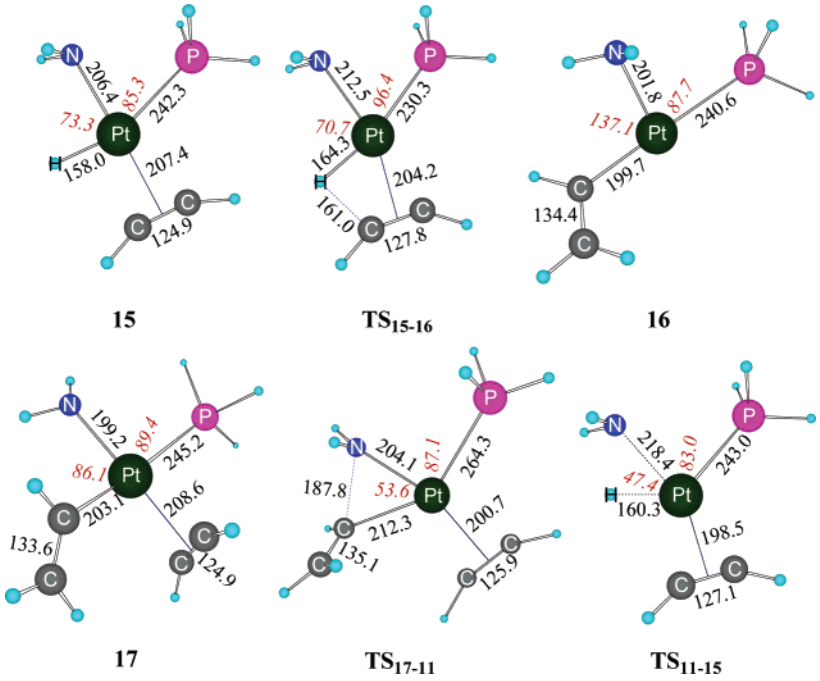

Figure 9. Equilibrium structures (bond lengths in pm, angles in deg) of the relevant stationary points in the PES of the catalytic cycle for the hydroamination of ethyne using model catalyst **7**, computed at the B3LYP/LANL2DZ+BSII(Pt)∪6-31G**(L) level of theory.

Table 3. Relative Energies, Enthalpies, Gibbs Free Energies, and Activation Barriers (kcal/mol) of the Hydroamination of Ethyne Catalyzed by Model "Catalyst" 7 Computed at the B3LYP/LANL2DZ+BSII(Pt)∪6-31G(L) and CCSD(T)/LANL2DZ+BSII(Pt)∪6-31G**(L)//B3LYP/LANL2DZ+BSII(Pt)∪6-31G**(L) Levels of Theory**

	ΔE_0	ΔH	ΔG	$\Delta E_{CCSD(T)}$	$\Delta E_0^{\ddagger}$ ($\Delta H^{\ddagger}$) [$\Delta G^{\ddagger}$]	$\Delta E_{CCSD(T)}^{\ddagger}$
			Hydroamination			
7 + ethyne	27.2	28.2	16.3	33.0		
15	0.00	0.00	0.00	0.00		
TS$_{15}$−16	8.5	8.1	9.2	10.5	8.5 (8.1) [9.2]	10.5
16	−12.3	−11.9	−13.7	−11.6		
17	−36.9	−37.4	−27.6	−44.7		
TS$_{17}$−11	−9.1	−9.6	−0.4	−9.3	27.8 (27.8) [27.2]	35.4
11 + product **C**	−53.7	−54.2	−56.2	−45.1		
11 + amine	−16.4	−15.3	−27.5	−8.5		
TS$_{11}$−15	13.6	13.7	13.0	17.0	30.0 (29.0) [28.5]	25.5

In the first stage of the catalytic cycle the ethyne molecule is coordinated to the "catalytically" active Pt(II) monomeric species, yielding the intermediate π-ethyne adduct, **15**. In this adduct the ethyne molecule occupies a *trans* position to the NH_2 ligand, adopting a coplanar orientation with respect to the coordination plane of the Pt(II) complex. The formation of intermediate **15** was calculated to be exoergic by −27.2 (−33.0) kcal/mol at the B3LYP (CCSD(T)) levels of theory. The inclusion of entropic effects (ΔG) reduces the exergonicity to −16.3 kcal/mol. It should be noted that the exoergicity of the first step of the hydroamination process is comparable to that of the hydrocyanation one.

Surprisingly the association of the ethyne molecule with the catalytic species **7** does not affect the Pt−H bond length, as was the case in the hydrosilylation and hydrocyanation processes. However, the Pt−N bond is lengthened by 5.3 pm, as a result of the *trans* influence of the ethyne ligand, while the Pt−P bond is shortened by 2.1 pm. These structural changes are reflected in the respective vibrational frequencies; the stretching vibrations of the Pt−H, Pt−N, and Pt−P bonds are predicted to be 2187, 556, and 231 cm^{-1}, respectively.

It should be noticed that the coordination of the ethyne molecule to the platinum center results in the lengthening of the C≡C triple bond by 4.3 pm, with a ν(C≡C) stretching vibrational frequency of 1856 cm^{-1}. The bending of the H−C≡C moiety of the coordinated ethyne molecule away from the Pt(II) center corresponds to a bending angle of 157.1°. Moreover, in the intermediate **15** the P−Pt−H bond angle deviates from linearity by 21.4°. The vibrational modes characterizing the coordination of the ethyne molecule with the Pt(II) metal center are the ν(Pt−C_2(centroid)) and ν_{as}(Pt−C_2) stretching vibrational modes that absorb at 368 and 440 cm^{-1}, respectively.

The σ(Pt−H) natural orbital is constructed from an $sd^{0.76}$ hybrid (43.07% d character) on the platinum atom, $h_{Pt} = -0.753(6s)_{Pt} + 0.646\ (5d_{xy})_{Pt} + 0.115(5d_{z^2})_{Pt}$, interacting in-phase with the 1s orbital on the bridging hydride, thus having the form $\sigma(Pt-H) = 0.697h_{Pt} + 0.717s_H$. Notice the decrease of the d character in the sd hybrid of Pt(II) with a concomitant increase of the s_H contribution to the σ(Pt−H) bonding interaction in **15** with respect to **12** and **8**. The Pt(II) metal center acquires a positive natural charge of 0.39 $|e|$, while the terminal hydride ligand acquires a negative natural charge of −0.10 $|e|$.

In the next step of the catalytic cycle insertion of ethyne into the Pt−H bond takes place, through **TS$_{15-16}$**, yielding intermediate **16**, with an activation barrier of 9.2 (10.5) kcal/mol in terms of $\Delta G^{\ddagger}$($\Delta E_{CCSD(T)}^{\ddagger}$). The activation barrier is comparable to that of the hydrosilylation process, but higher than the corresponding activation barrier of the hydrocyanation one. The structural features of the transition state **TS$_{15-16}$** are similar to those of **TS$_{8-9}$** and **TS$_{12-13}$**. The distance between the migrating hydride ligand and the nearest acceptor C atom of the ethyne ligand has dramatically shortened by 73.9 pm with respect to

the corresponding distance in complex **15**. The Pt−C(centroid) distance in $\mathbf{TS_{15-16}}$ is shortened by 3.2 pm, while the C−C bond distance of the coordinated ethyne molecule is further lengthened by 2.9 pm with respect to intermediate **15**. In the vibrational mode corresponding to the imaginary frequency of $\mathbf{TS_{15-16}}$, $\nu_i = 730$ cm^{-1}, the dominant motions involve the transferring hydride along with the nearest acetylenic H atom of the coordinated H−C≡C−H molecule. The ethenyl intermediate **16** is 12.3 (11.6) kcal/mol in terms of ΔE_0 more stable than intermediate **15** at the B3LYP (CCSD(T)) levels. **16** is a coordinatively unsaturated 14*e* Pt(II) complex with a T-shaped structure (∠C−Pt−P = 177.6°) and a N−Pt−C−C torsion angle of −125.7°.

The subsequent step of the catalytic cycle involves coordination of a second ethyne molecule to the Pt(II) center of intermediate **16**, yielding the coordinatively unsaturated 16*e* Pt(II) complex **17**, which via a reductive elimination process affords the product **C** ($H_2C{=}CHNH_2$) and the catalytic species **11**. Upon oxidative addition of H−NH_2 to intermediate **11**, the catalytic species **12** is regenerated and the catalytic cycle is completed. During the course of the reductive elimination process the amine group is transferred to the acceptor C atom of the coordinated ethenyl group via the transition state $\mathbf{TS_{17-11}}$, surmounting a relatively high activation barrier of 27.8 (35.4) kcal/mol. The reductive elimination in hydroamination is predicted to be exoergic at the B3LYP level ($\Delta E_0 = -16.8$ kcal/mol) and almost thermoneutral ($\Delta E_0 = -0.4$ kcal/mol) at the CCSD(T) level. In $\mathbf{TS_{17-11}}$ the amine ligand is inclined toward the ethenyl group by 36.4° (N−Pt−C = 53.6°). The distance between the migrating cyanide ligand and the nearest C atom of the acceptor ethenyl group is 48.2 pm longer than the C−N bond length in the final product **C**, whereas the C−C bond distance is only 1.1 pm longer than the respective C−C bond length of product **C**. In the vibrational mode corresponding to the imaginary frequency of $\mathbf{TS_{17-11}}$, $\nu_i = 513$ cm^{-1}, the dominant motions involve the transferring cyanide group along with the nearest C atom of the $H_2C{=}CH-$ ligand.

Finally, the oxidative addition of H−NH_2 to the coordinatively unsaturated 14*e* Pt(0) complex **11**, regenerating the "true" catalytic species **15**, corresponds to an endothermic process, with endothermicity of 16.4 (8.5) kcal/mol at the B3LYP (CCSD(T)) levels, and surmounts a remarkably high activation barrier of 28.5 (25.5) kcal/mol in terms of $\Delta G^{\ddagger}(\Delta E_{CCSD(T)}^{\ddagger})$. These activation barriers are much higher than the corresponding oxidative addition barriers of the hydrosilylation and hydrocyanation processes. The transition state $\mathbf{TS_{11-15}}$ involves a loosely associated H−NH_2 molecule interacting with the Pt(0) metal center in a κ^2-N,H bonding mode, but with the N−H bond strongly weakened. In the vibrational mode corresponding to the imaginary frequency of $\mathbf{TS_{10-12}}$, $\nu_i = 925$ cm^{-1}, the dominant motion involves the dissociation of the coordinated N−H bond and the formation of the Pt−H and Pt−N bonds.

In summary the geometric and energetic profile of the hydroamination of ethyne catalyzed by the hydrido-bridged diplatinum complexes closely resembles those of the respective hydrosilylation and hydrocyanation reactions. However, the hydroamination process is less favored both thermodynamically and kinetically, since the two critical rate-limiting steps, namely, the reductive elimination and the oxidative addition steps, are less favored. Therefore the hydrido-bridged diplatinum complexes are predicted to be less efficient catalysts for hydroamination of unsaturated substrates. This is further substantiated by the computed δE values of 67.3 (62.1) at the B3LYP (CCSD(T)) levels, which are higher than those of the hydrosilylation and hydrocyanation processes. This could be due to the stabilization of the lowest energy species in the cycle of the hydroamination process. It should be noted that the predicted mechanism of the hydroamination of ethyne catalyzed by the hydrido-bridged diplatinum complexes differs significantly from the suggested mechanism for the intermolecular hydroamination of alkynes catalyzed by organolanthanide complexes.[34]

Concluding Remarks

A detailed investigation of the mechanism of hydrosilylation, hydrocyanation, and hydroamination of ethyne catalyzed by hydrido-bridged diplatinum complexes has been carried out in the framework of electronic structure calculations at the B3LYP and CCSD(T) levels of theory, using the LANL2DZ+BSII(Pt)∪6-31G**(L) basis set.

The present investigation examines, in terms of located structures, energies, and activation barriers, the participation of postulated intermediates. Prior qualitative mechanistic assumptions are substituted by the presented theoretically well-founded and detailed analysis of both the thermodynamic and kinetic aspects that substantially improve the insight into the reaction course and enlarge them with novel mechanistic proposals.

Our calculations show that the catalytically "active" species are the 16*e* coordinatively unsaturated mononuclear [Pt(L)(H)-$(PH_3)(\eta^2$-$C_2H_2)$] (L = SiH_3, CN, NH_2) species resulting upon dissociation of the hydrido-bridged dinuclear [{Pt(L)(μ-H)-$(PH_3)\}_2$] precursors promoted by the incoming unsaturated substrate.

Overall, the catalytic cycle involves three critical rate-limiting steps, corresponding to (i) the hydride migration to the acceptor C atom of the coordinated ethyne substrate, (ii) the reductive elimination of the hydrosilylated, hydrocyanated, or hydroaminated product, and (iii) the oxidative addition process that regenerates the catalytic species. The computed activation barriers ($\Delta E_{CCSD(T)}^{\ddagger}$) for the rate-determining steps were found to be 11.6, 5.1, and 7.1 kcal/mol for the hydrosilylation, 6.9, 24.9, and 1.6 kcal/mol for the hydrocyanation, and 10.5, 35.5, and 25.5 kcal/mol for the hydroamination reactions. The rate-limiting steps differ in the three catalytic processes, being step (i) in hydrosilylation, step (ii) in hydrocyanation, and both steps (ii) and (iii) in hydroamination. The efficiency of the catalytic cycles determined by the energy span quantity, δE, follows the trend hydrocyanation ≥ hydrosilylation > hydroamination. Moreover, the hydosilylation, hydrocyanation, and hydroamination of ethyne catalyzed by the hydrido-bridged diplatinum catalysts are predicted to be exothermic by −32.1 (−25.5), −37.8 (−28.2), and −53.7 (−45.1) kcal/mol, respectively, at the B3LYP (CCSD(T)) levels of theory, in line with the experimental observations in the case of hydrosilylation.

Supporting Information Available: Complete ref 12. The Cartesian coordinates and energies of all stationary points are compiled in Tables S1 and S2, respectively. This information is available free of charge via the Internet at http://pubs.acs.org.

OM0509342

(34) (a) Ryu, J.-S.; Li, G. Y.; Marks, T. J. *J. Am. Chem. Soc.* **2003**, *125*, 12584−12605. (b) Matta, A.; Lanza, G.; Fragala, I. L.; Marks, T. J. *Organometallics* **2004**, *23*, 4097−4104.